Acoustic Time-Reversal Mirrors

Mathias Fink

Laboratoire Ondes et Acoustique, Ecole Supérieure de Physique et de Chimie Industrielle de la Ville de Paris, Université Denis Diderot,
UMR CNRS 7587, 10 Rue Vauquelin, 75005 Paris, France
mathias.fink@espci.fr

Abstract. The objective of this paper is to show that time-reversal invariance can be exploited in acoustics to accurately control wave propagation through complex media.

1 Introduction

In time-reversal acoustics [1,2,3,4] a signal is recorded by an array of transducers, time-reversed and then re-transmitted into the medium. The re-transmitted signal propagates back through the same medium and refocuses on the source. In a time-reversal cavity (TRC) the array completely surrounds the source, and thus the time-reversed signals propagate backwards through the medium and go through all the multiple scattering, reflections and refraction that they underwent in the forward direction. If the time-reversal operation is only performed on a limited angular area (a time-reversal mirror TRM), a small part of the field radiated by the source is captured and time-reversed, thus limiting reversal and focusing quality.

The basic principles and limitations of time-reversal acoustics are described in Sect. 2. Various time-reversal experiments conducted with TRMs are then discussed in Sect. 3. It will be shown that focusing quality is improved if the wave traverses random media or if the wave propagates in media with reflecting boundaries as waveguides or reverberating cavities. The focusing resolution may be much better than the resolution obtained in an homogeneous medium. Multiple scattering or multiple reflections allow one part of the initial wave to be redirected towards the TRM that normally misses the transducer array. TRM appears to have an aperture that is much larger than its physical size. It will be shown that, for a reflecting cavity with chaotic boundaries, a one-channel TRM is sufficient to ensure optimal focusing. Then differences between time reversal and phase conjugation are discussed. Finally, Sect. 4 includes a short description of the potential of TRM in various applications (medical therapy and non-destructive testing).

2 Time-Reversal Cavities and Mirrors

The basic theory employs a scalar wave formulation, $\phi(\boldsymbol{r}, t)$, and, hence, is strictly applicable to acoustic or ultrasound propagations in fluid. However,

Fink et al. (Eds.): Imaging of Complex Media with Acoustic and Seismic Waves,
Topics Appl. Phys. **84**, 17–43 (2002)

the basic ingredients and conclusions apply equally well to elastic waves in a solid and to electromagnetic fields.

In any propagation experiment, the acoustic sources and the boundary conditions determine a unique solution, $\phi(\boldsymbol{r}, t)$, in the fluid. The goal, in time-reversal experiments, is to modify the initial conditions in order to generate the dual solution $\phi(\boldsymbol{r}, T - t)$, where T is a delay due to causality requirements. *Jackson* and *Cassereau* [4,5] have studied theoretically the conditions necessary to insure the generation of $\phi(\boldsymbol{r}, T - t)$ in the entire volume of interest.

2.1 The Time-Reversal Cavity

From an experimental point of view a TRC consists of a two-dimensional piezoelectric transducer array that samples the wavefield over a closed surface. An array pitch of the order of $\lambda/2$, where λ is the smallest wavelength of the pressure field, is needed to insure the recording of all the information on the wavefield. Each transducer is connected to its own electronic circuitry, which consists of a receiving amplifier, an analog-to-digital converter, a storage memory and a programmable transmitter able to synthesize a time-reversed version of the stored signal. Although reversible acoustic retinas usually consist of discrete elements, it is convenient to examine the behavior of idealized continuous retinas, defined by two-dimensional surfaces. In the case of a TRC, we assume that the retina completely surrounds the source. The basic time-reversal experiment can be described in the following way:

As a first step, a point-like source located at $\boldsymbol{r}_0$ inside a volume V surrounded by the retina surface S emits a pulse at $t = t_0 \geq 0$. The wave equation in a medium of density $\rho(\boldsymbol{r})$ and compressibility $\kappa(\boldsymbol{r})$ is given by

$$(L_\mathrm{r} + L_\mathrm{t})\phi(\boldsymbol{r}, t) = -A\delta(\boldsymbol{r} - \boldsymbol{r}_0)\delta(t - t_0)\,,$$
$$L_\mathrm{r} = \nabla\left(\frac{1}{\rho(\boldsymbol{r})}\nabla\right)\,, \quad L_\mathrm{t} = -\kappa(\boldsymbol{r})\partial_{tt}\,, \tag{1}$$

where A is a dimensional constant that insures the compatibility of physical units between the two sides of the equation; for simplicity, this constant will be omitted in the following. The solution to (1) reduces to the Green's function $G(\boldsymbol{r}, t|\boldsymbol{r}_0, t_0)$. Classically, $G(\boldsymbol{r}, t|\boldsymbol{r}_0, t_0)$ is written as a diverging spherical wave (homogeneous and free space case) and additional terms that describe the interaction of the field itself with the inhomogeneities (multiple scattering) and the boundaries.

We assume that we are able to measure the pressure field and its normal derivative at any point on the surface S during the interval $[0, T]$. As time-reversal experiments are based on a two-step process, the measurement step must be limited in time by a parameter T. In all the following, we assume that the contribution of multiple scattering decreases with time and that T

is chosen such that the information loss can be considered to be negligible inside the volume V.

During the second step of the time-reversal process, the initial source at $\boldsymbol{r}_0$ is removed, and we create on the surface of the cavity monopole and dipole sources that correspond to the time reversal of those same components measured during the first step. The time-reversal operation is described by the transform $t \to T - t$ and the secondary sources are

$$\begin{cases} \phi_{\mathrm{s}}(\boldsymbol{r}, t) = G(\boldsymbol{r}, T - t | \boldsymbol{r}_0, t_0), \\ \partial_{\mathrm{n}} \phi_{\mathrm{s}}(\boldsymbol{r}, t) = \partial_{\mathrm{n}} G(\boldsymbol{r}, T - t | \boldsymbol{r}_0, t_0) . \end{cases} \tag{2}$$

In this equation, ∂_{n} is the normal derivative operator with respect to the normal direction $\boldsymbol{n}$ to S, oriented outward. Due to these secondary sources on S, a time-reversed pressure field $\phi^{\mathrm{tr}}(\boldsymbol{r}_1, t_1)$ propagates inside the cavity. It can be calculated using a modified version of the Helmoltz–Kirchhoff integral:

$$\begin{aligned} \phi^{\mathrm{tr}}(\boldsymbol{r}_1, t_1) = \int_{-\infty}^{+\infty} \mathrm{d}t \iint_S [& G(\boldsymbol{r}_1, t_1 | \boldsymbol{r}, t) \partial_{\mathrm{n}} \phi_{\mathrm{s}}(\boldsymbol{r}, t) \\ & - \phi_{\mathrm{s}}(\boldsymbol{r}, t) \partial_{\mathrm{n}} G(\boldsymbol{r}_1, t_1 | \boldsymbol{r}, t)] \frac{\mathrm{d}^2 \boldsymbol{r}}{\rho(\boldsymbol{r})} . \end{aligned} \tag{3}$$

Spatial reciprocity and time-reversal invariance of the wave equation (1) yield the following expression:

$$\phi^{\mathrm{tr}}(\boldsymbol{r}_1, t_1) = G(\boldsymbol{r}_1, T - t_1 | \boldsymbol{r}_0, t_0) - G(\boldsymbol{r}_1, t_1 | \boldsymbol{r}_0, T - t_0) . \tag{4}$$

This equation can be interpreted as the superposition of incoming and outgoing spherical waves centered on the initial source position. The incoming wave collapses at the origin and is always followed by a diverging wave. Thus the time-reversed field, observed as a function of time, from any location in the cavity, shows two wavefronts, the second one being an exact replica of the first, but multiplied by -1.

If we assume that the retina does not perturb the propagation of the field (free-space assumption) and that the acoustic field propagates in an homogeneous fluid, the free-space Green's function G reduces to a diverging spherical impulse wave that propagates with a sound speed c. Introducing its expression in (4) yields the following formulation of the time-reversed field:

$$\phi^{\mathrm{tr}}(\boldsymbol{r}_1, t_1) = K(\boldsymbol{r}_1 - \boldsymbol{r}_0, t_1 - T + t_0) , \tag{5}$$

where the kernel distribution $K(\boldsymbol{r}, t)$ is given by

$$K(\boldsymbol{r}, t) = \frac{1}{4\pi |\boldsymbol{r}|} \delta \left(t + \frac{|\boldsymbol{r}|}{c} \right) - \frac{1}{4\pi |\boldsymbol{r}|} \delta \left(t - \frac{|\boldsymbol{r}|}{c} \right) . \tag{6}$$

The kernel distribution $K(\boldsymbol{r}, t)$ corresponds to the difference between two impulse spherical waves one converging to and one diverging from the origin of the spatial coordinate system, i.e., the location of the initial source.

Resulting from this superposition, the pressure field remains finite for all time throughout the cavity, although the converging and diverging spherical waves show a singularity at the origin. Note that this singularity occurs at time $t_1 = T - t_0$.

The time-reversed pressure field, observed as a function of time, shows two wavefronts, the second one being an exact replica of the first, but multiplied by -1. If we consider a wide-band excitation function instead of a Dirac distribution, $\delta(t)$, the two wavefronts overlap near the focal point, therefore resulting in a temporal distortion of the acoustic signal. It can be shown that this distortion yields a temporal derivation of the initial excitation function at the focal point.

If we now calculate the Fourier transform of (6) over the time variable t, we obtain

$$\tilde{K}(\boldsymbol{r},\omega) = \frac{1}{2\mathrm{j}\pi}\frac{\sin\left(\omega\left|\boldsymbol{r}\right|/c\right)}{\left|\boldsymbol{r}\right|} = \frac{1}{\mathrm{j}\lambda}\frac{\sin\left(k\left|\boldsymbol{r}\right|\right)}{k\left|\boldsymbol{r}\right|}\,, \tag{7}$$

where λ and k are the wavelength and wavenumber, respectively. As a consequence, the time-reversal process results in a pressure field that is effectively focused on the initial source position, but with a focal spot size limited to one half-wavelength. The size of the focal spot is a direct consequence of the superposition of the two wavefronts and can be interpreted in terms of the diffraction limitations (loss of the evanescent components of the acoustic fields).

A similar interpretation can be given in the case of an inhomogeneous fluid, but the Green's function G now takes into account the interaction of the pressure field with the inhomogeneities of the medium. If we were able to create a film of the propagation of the acoustic field during the first step of the process, the final result could be interpreted as a projection of this film in the reverse order, immediately followed by a re-projection in the initial order.

The apparent failure of the time-reversed operation that leads to diffraction limitation can be interpreted in the following way: The second step described above is not strictly the time reversal of the first step. During the second step of an ideal time-reversed experiment, the initial active source (which injects some energy into the system) must be replaced by a *sink* (the time reversal of a source). An acoustic sink is a device that absorbs all arriving energy without reflecting it. De Rosny and Fink, using the source as a diverging wavefront canceller, have recently built such a sink in our laboratory and have observed a focal spot size quite below diffraction limits [6].

2.2 The Time-Reversal Mirror

This theoretical model of the closed time-reversal cavity is interesting, since it affords an understanding of the basic limitations of the time-reversed self-focusing process; but it has some limitations, particularly compared to an experimental setup:

- It can be proven that it is not necessary to measure and time-reverse both the scalar field (acoustic pressure) and its normal derivative on the cavity surface; measuring the pressure field and re-emitting the time-reversed field in the backward direction yields the same results, on the condition that the evanescent parts of the acoustic fields have vanished (propagation along several wavelengths) [7]. This comes from the fact that each transducer element of the cavity records the incoming field from the forward direction and retransmits it (after the time-reversal operation) in the *backward* direction (and not in the forward direction). The change between the forward and backward directions replaces the measurement and the time reversal of the field-normal derivative.
- From an experimental point of view, it is not possible to measure and re-emit the pressure field at any point on a 2-dimensional surface; experiments are carried out with transducer arrays that spatially sample the receiving and emitting surface. The spatial sampling of the TRC by a set of transducers may introduce grating lobes. These lobes can be avoided by using an array pitch smaller than $\lambda_{\min}/2$, where $\lambda_{\min}$ is the smallest wavelength of the transient pressure field. In this case, each transducer senses all the wavevectors of the incident field.
- The temporal sampling of the data recorded and transmitted by the TRC has to be at least of the order of $T_{\min}/8$ ($T_{\min}$ is the minimum period) to avoid secondary lobes [8].
- It is generally difficult to use acoustic arrays that completely surround the area of interest, and the closed cavity is usually replaced by a TRM of finite angular aperture. This yields an increase in the point spread function dimension that is usually related to the mirror angular aperture observed from the source.

3 Time-Reversal Experiments

3.1 Time Reversal through Random Media

Derode et al. [9] carried out the first experimental demonstration of the reversibility of an acoustic wave propagating through a random collection of scatterers with strong multiple-scattering contributions. In an experiment such as the one depicted in Fig. 1, a multiple-scattering sample is placed between the source and an array made of 128 elements. The whole setup is in a water tank. The scattering medium consists of a set of 2000 parallel steel rods (diameter 0.8 mm) randomly distributed. The sample thickness is $L = 40$ mm, and the average distance between rods is 2.3 mm. The source is 30 cm away from the TRM and transmits a short (1 µs) ultrasonic pulse (3 cycles of a 3.5 MHz, Fig. 2a). Figure 2b shows the waveform received on the TRM by one of the elements. It spread over 250 µs, i.e., ~ 250 times the initial pulse duration. A long incoherent wave is observed, which results

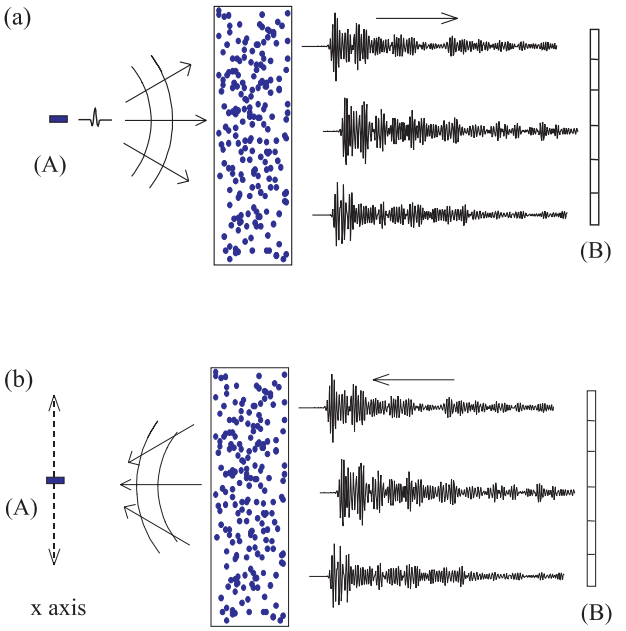

Fig. 1. Sketch of experiment **(a)** first step, the source sends a pulse through the sample, the transmitted wave is recorded by the TRM. **(b)** second step, the multiplay scattered signals are time reversed, they are retransmitted by the TRM and A records the reconstructed pressure field

from the multiply scattered contribution. As a second step to the experiment, the 128 signals are time-reversed and transmitted and an hydrophone measures the time-reversed wave around the source location. Two different aspects of this problem have been studied: the property of the signal recreated at the source location (time compression) and the spatial property of the time-reversed wave around the source location (spatial focusing).

The time-reversed wave traverses the rods back to the source, and the signal received at the source is represented in Fig. 2c; an impressive compression is observed, since the received signal lasts about 1 μs, in comparison to 250μs. The pressure field is also measured around the source, in order to obtain the directivity pattern of the beam emerging from the rods after time reversal, and the results are plotted in Fig. 3. Surprisingly, multiple scattering has *not* degraded the resolution of the system; indeed, the resolution is found to be six times finer (thick line) than the classical diffraction limit (thin line). However, this effect does not contradict the laws of diffraction. The intersection of the incoming wavefront with the sample has a typical size D. After time reversal, the waves travel on the same scattering paths and focus back on the source as if they were passing through a converging lens with size D. The angular aperture of this pseudo-lens is much wider than

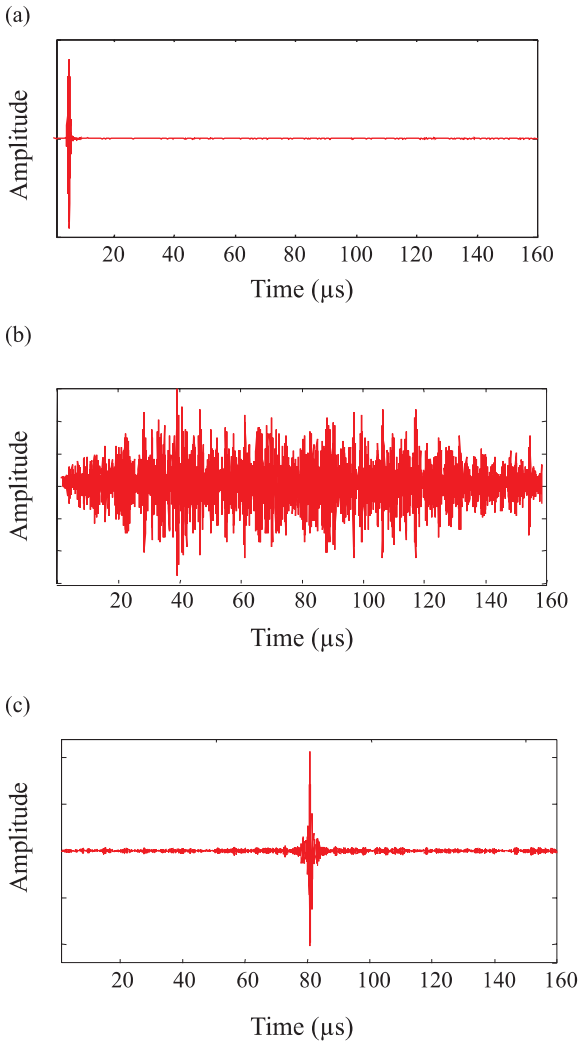

Fig. 2. **(a)** Signal transmitted in water and recieved on transducer 64. **(b)** Signal transmitted through the multiple scattering sample and recieved on transducer 64. **(c)** Signal recieved on the source

that of the array alone, and hence there is an improvement in resolution. In other words, because of the scattering sample, the array is able to detect higher spatial frequencies than it would in a purely homogeneous medium. High spatial frequencies that would have been otherwise lost are redirected towards the array, due to the presence of the scatterers in a large area.

This experiment also shows that the acoustic time-reversal experiments are surprisingly stable. The recorded signals are sampled with 8-bit analog-to-

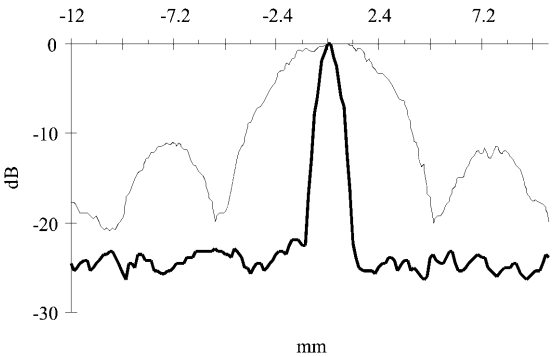

Fig. 3. Directivity patterns in water (*thin line*), through the multiple scattering medium (*thick line*)

digital converters that introduce quantization errors, but the focusing process still works. This has to be compared to time-reversal experiments involving particles moving like balls on an elastic billiard table of the same geometry. Computation of the direct and reversed particle trajectories moving in a plane among a fixed array of some thousand obstacles shows that the complete trajectory is irreversible. Indeed, such a system is a well-known example of a chaotic system that is highly sensitive to initial conditions. The finite precision that occurs in the computer leads to an error in the trajectory of the time-reversed particle that grows exponentially with the number of scattering encounters.

Recently, *Snieder* and *Scales* [10] performed numerical simulations to point out the fundamental difference between waves and particles in the presence of multiple scattering by random scatterers. In fact, they used time reversal as a diagnostic of wave and particle chaos; in a time-reversal experiment, complete focusing on the source will only take place if the velocity and positions are known exactly. The degree δ to which errors in these quantities destroy the quality of focusing is diagnostic of the stability of the wave or particle propagation. Intuitively, the consequences of a slight deviation δ in the trajectory of a billiard ball will become more and more obvious as time goes on and as the ball undergoes more and more collisions. Waves are much less sensitive than particles to initial conditions. In a multiple-scattering situation, the critical length scale δ that causes a significant deviation at a time t in the future decreases exponentially with time in the case of particles, whereas it only decreases as the square root of time for waves in the same situation.

Waves and particles react in fundamentally different ways to perturbations of the initial conditions. The physical reason for this is that each particle follows a well-defined trajectory, whereas waves travel along all possible trajectories, visiting all the scatterers in all possible combinations. While a small error in the initial velocity or position makes the particle miss one obstacle and completely change its future trajectory, the wave amplitude is

much more stable because it results from the interference of all the possible trajectories; small errors in the transducer operations will sum up in a linear way for wave propagation resulting in only a small perturbation.

3.1.1 Time Reversal as a Time Correlator

As for any linear and time-invariant process, wave propagation through a multiple-scattering medium may be described as a linear system with different impulse responses. If a source located at $\boldsymbol{r}_0$ sends a Dirac pulse $\delta(t)$, the jth transducer of the TRM will record the corresponding impulse response $h_j(t)$ for a point transducer located at $\boldsymbol{r}_j$ to the Green function $G(\boldsymbol{r}_j, t|\boldsymbol{r}_0, 0)$. Moreover, due to reciprocity, $h_j(t)$ is also the impulse response describing the propagation of a pulse from the jth transducer to the source. Thus, neglecting the causal time delay T, the time-reversed signal at the source is equal to the convolution product $h_j(t) * h_j(-t)$.

This convolution product, in terms of signal analysis, is typical of a *matched filter*. Given a signal as input, a matched filter is a linear filter whose output is optimal in some sense. Whatever the impulse response $h_j(t)$, the convolution $h_j(t) * h_j(-t)$ is maximum at time $t = 0$. This maximum is always positive and equals $\int h_j^2(t)\mathrm{d}t$, i.e., the energy of the signal $h_j(t)$. This has an important consequence. Indeed, with an array of N elements, the time-reversed signal recreated on the source writes as a sum:

$$\phi^{\mathrm{tr}}(\boldsymbol{r}, t) = \sum_{j=1}^{j=N} h_j(t) * h_j(-t)\,. \tag{8}$$

Even if $h_j(t)$ are completely random and apparently uncorrelated signals, each term in this sum reaches its maximum at time $t = 0$. Therefore, all contributions add constructively around $t = 0$, whereas at earlier or later times uncorrelated contributions tend to destroy one another. Thus the re-creation of a sharp peak after time reversal in an array of N elements can be viewed as an interference process between the N outputs of N matched filters.

The robustness of the TRM can also be accounted for through the matched filter approach. If, for some reason, the TRM does not exactly retransmit $h_j(-t)$ but rather $h_j(-t) + n_j(t)$, where $n_j(t)$ is an additional noise on channel j, then the re-created signal is written as follows:

$$\sum_{j=1}^{j=N} h_j(t) * h_j(-t) + \sum_{j=1}^{j=N} h_j(t) * n(t)\,.$$

The time-reversed signals $h_j(-t)$ are tailored to exactly match the medium impulse response, which results in a sharp peak. However, an additional small noise is not matched to the medium and, given the extremely long duration involved, it generates a low-level, long-lasting background noise instead of a sharp peak.

3.1.2 Time Reversal as a Spatial Correlator

Another way to consider the focusing properties of the time-reversed wave is to follow the impulse response approach and treat the time-reversal process as a spatial correlator. If we consider $h_j^{'}(t)$ to be the propagation impulse response from the jth element of the array to an observation point $\boldsymbol{r}_1$, not the source location $\boldsymbol{r}_0$, the signal recreated at $\boldsymbol{r}_1$ at time $t_1 = 0$ can be written:

$$\phi_j^{\mathrm{tr}}(\boldsymbol{r}_1, 0) = \int h_j(t) h_j^{'}(t) \mathrm{d}t \tag{9}$$

Notice that this expression can be used as a way to define the directivity pattern of the time-reversed waves around the source. Now, due to reciprocity, the source S and the receiver can be exchanged, i.e., $h_j^{'}(t)$ is also the signal that would be received at $\boldsymbol{r}_1$ if the source was the jth element of the array. Therefore, we can imagine that this array element is the source and that the transmitted field is observed at two points $\boldsymbol{r}_1$ and $\boldsymbol{r}_0$. The spatial correlation function of this wavefield would be $\left\langle h_j(t) h_j^{'}(t) \right\rangle$, where the impulse-response product is averaged over different realizations of the disorder. Therefore, (9) can be viewed as an estimator of this spatial correlation function. Note that in one time-reversal experiment we have only access to a single realization of the disorder. However, the ensemble average can be replaced by a time average, a frequency average or a spatial average over a set of transducers. In that sense, the spatial resolution of the TRM (i.e., the $-6\,\mathrm{dB}$ width of the directivity pattern) is simply an estimate of the correlation length of the scattered wavefield [11].

This has an important consequence. Indeed, if the resolution of the system essentially depends on correlation properties of the scattered wavefield, it should become independent from the array's aperture. This is confirmed by the experimental results. Figure 4 presents the directivity patterns obtained

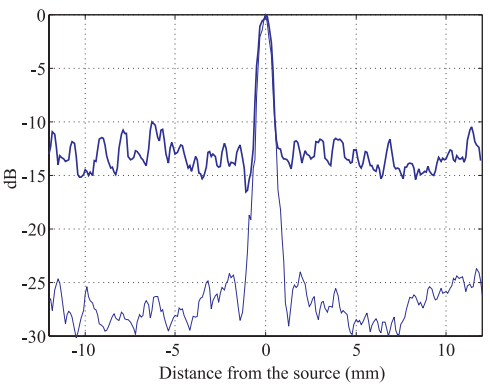

Fig. 4. Directivity patterns with $N = 122$ transducers (*thin line*) and $N = 1$ transducer (*thick line*)

through a 40-mm-thick multiple-scattering sample, using either one array element or the whole array (122 elements) as a TRM. In both cases, the spatial resolution at $-6\,\mathrm{dB}$ is the same: $\sim 0.85\,\mathrm{mm}$. In contrast to what happens in a homogeneous medium, enlarging the aperture of the array does not change the $-6\,\mathrm{dB}$ spatial resolution. However, even though the number N of active array elements does not influence the typical width of the focal spot, it has a strong impact on the background level of the directivity pattern ($\sim -12\,\mathrm{dB}$ for $N = 1$, $\sim -28\,\mathrm{dB}$ for $N = 122$), as can be seen in Fig. 4.

Finally, the fundamental properties of time reversal in a random medium rely on the fact that it is both a space and time correlator, and the time-reversed waves can be viewed as an estimate of the space and time auto-correlation functions of the waves scattered by a random medium. The estimate becomes better as the number of transducers in the mirror is increased.

Moreover, the system is not sensitive to a small perturbation, since adding a small noise to the scattered signals (e.g., by digitizing them on a reduced number of bits) may alter the noise level but does not drastically change the correlation time or the correlation length of the scattered waves. Even in the extreme case where the scattered signals are digitized *on a single bit*, Derode has shown recently that the time and space resolution of the TRM were practically unchanged [12], which is striking evidence for the robustness of wave time reversal in a random medium.

3.2 Time Reversal in Waveguides

In the time-reversal cavity approach, the transducer array samples a closed surface surrounding the acoustic source. In the last section, we saw how the multiple-scattering processes in a large sample widen the effective TRM aperture. The same kind of improvement may be obtained for waves propagating in a waveguide or in a cavity. Multiple reflections along the medium boundaries significantly increase the apparent aperture of the TRM. The basic idea is to replace one part of the TRC transducers by reflecting boundaries that redirect one part of the incident wave towards the TRM aperture. Thus spatial information is converted into the time domain and the reversal quality depends crucially on the duration of the time-reversal window, i.e., the length of the recording to be reversed.

3.2.1 Ultrasonic Waveguide

Experiments conducted by Roux in rectangular ultrasonic waveguides have shown the effectiveness of time-reversal processing in compensating for multipath effects [13]. The experiment is conducted in a waveguide whose interfaces are plane and parallel. The length of the guide is $L \approx 800\,\mathrm{mm}$ along the y axis, with a vertical water depth $H \approx 40\,\mathrm{mm}$ along the x axis.

A point-like ultrasonic source is located on one side of the waveguide. On the other side, a TRM, identical to the one used in the multiple-scattering

medium, is used. Ninety-six of the array elements are used, which corresponds to an array aperture equal to the waveguide aperture.

Figure 5a shows the field radiated by the source and recorded by the transducer array after propagation through the channel. After the arrival of the first wavefront corresponding to the direct path, we observe a set of signals, due to multiple reflections of the incident wave between the interfaces, that spread over 100μs. Figure 5b represents the signal received on one transducer of the TRM.

After the time-reversal operation of the 100μs signals, we observe the spatio-temporal distribution of the time-reversed field on the source plane (Fig. 6a) and we note a remarkable temporal compression at the source location (Fig. 6b). This means that multipath effects are fully compensated for. The signal observed at the source is nearly identical to the one received in a time-reversed experiment conducted in free space.

In this experiment, the transfer function of the waveguide has been completely compensated for by the time-reversal process. As with a multiple-scattering medium, the time-reversal process enables the realization of an

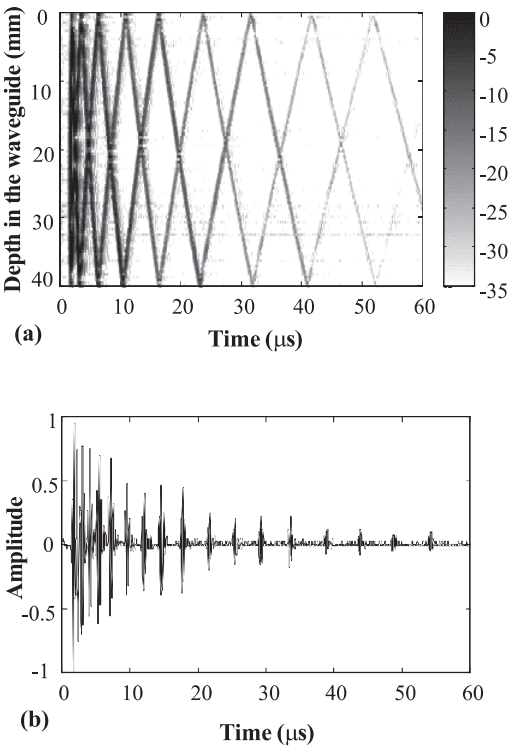

Fig. 5. **(a)** Field radiated by the source and recorded by the transducer array after propagation through the channel. **(b)** Signal recieved on one transducer of the TRM

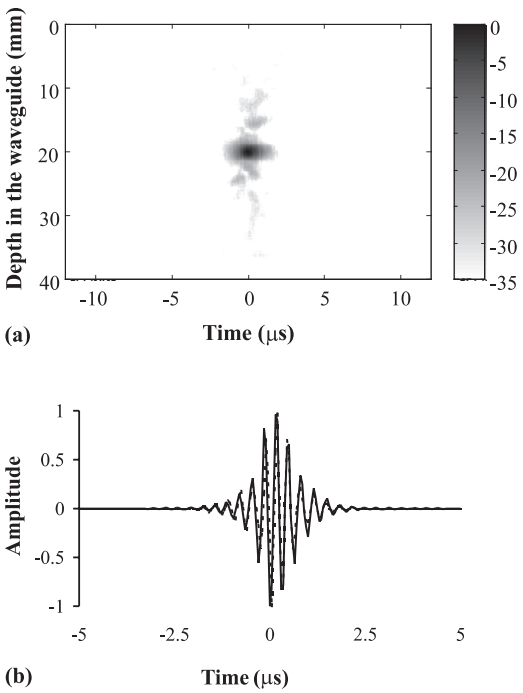

Fig. 6. **(a)** Spatio-temporal distribution of the time-reversed field on the source plane. **(b)** Temporal compression at the source location

optimal matched filter of the waveguide transfer function. Analysis of Fig. 6 shows that the ratio between the peak signal and the side lobe level is on the order of 45 dB.

Figure 7 shows the directivity pattern of the time-reversed field observed in the source plane. The time-reversed field is focused on a spot which is much smaller than the one obtained with the same TRM in free space. In our experiment, the −6 dB lateral resolution is improved by a factor of 9. This can be easily interpreted by the images theorem in a medium bounded by two mirrors. For an observer located at the source point, the 40 mm TRM appears to be accompanied by a set of virtual images related to multipath reverberation. The effective TRM is then a set of TRMs as shown in Fig. 8. When taking into account the first 10 arrivals, the theoretical effective aperture of the mirror array is 10 times larger than the real aperture. However, in practice, as the replicas arrive later, their amplitudes decrease. The angular directivity of the transducers leads to an apodization of the effective aperture of the TRM.

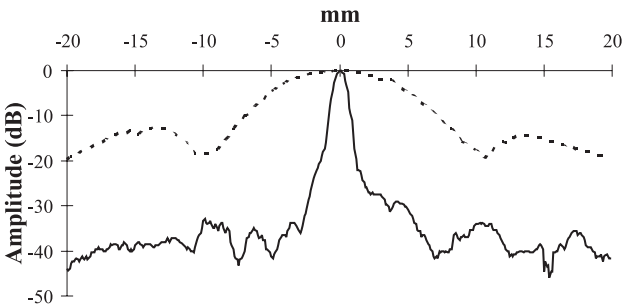

Fig. 7. Directivity pattern of the time-reversed field observed in the source plane in free space (*dotted line*), in the waveguide (*solid line*)

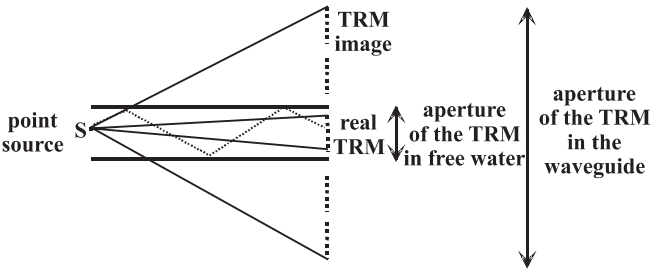

Fig. 8. Due to reverberation in the waveguide, the effective aperture of the TRM is increased

3.2.2 Underwater Acoustics

Acoustic waveguides are currently found in underwater acoustics, especially in shallow water, where multipath propagation limits the capacity of underwater communication systems. The problem arises because acoustic transmission in shallow water bounces off the ocean surface and floor, so that a transmitted pulse gives rise to multiple arrivals at the receiver.

To compensate for acoustic reverberation in the ocean, one-channel time reversal was first introduced in the early 1960s by *Parvulescu* and *Clay* [14,15]. They performed experiments in shallow water at sea with one transducer working in a time-reversed mode. They observed temporal compression but their experiments did not include the spatial focusing property of TRMs. Parvulescu's approach consists of considering the ocean as a correlator. *Jackson* and *Dowling* [4] developed a theoretical formalism to describe phase conjugation in the ocean. This formalism is based on the modal decomposition of the pressure field in an acoustic waveguide. Following this approach, in 1992 *Feuillade* and *Clay* [16] carried out numerical time-reversal experiments in shallow water. Since 1996, *Kuperman* et al. [17,18] have performed several underwater acoustics experiments in a 120-m-deep ocean waveguide. At frequencies of 500 Hz and 3.5 kHz, they used a 24-element TRM to accomplish time-reversal focusing and multipath compensation from 7 km up to 30 km.

Theoretically speaking, for one spectral component at frequency ω, the time-reversal operation consists of a phase conjugation of the incident field. For an incident field coming from a point source located at depth x_s in the plane $y = L$, the phase conjugation, performed in shallow water, from a vertical array of N discrete sources located in the plane $y = 0$ leads to the following time-reversed pressure field at observation point (x, y):

$$\phi^{\mathrm{tr}}(x,y,t) = \sum_{j=1}^{N} G_\omega\left(x,y|x_j,0\right) G_\omega^*\left(x_j,0|x_\mathrm{s},L\right) \exp\left(-\mathrm{i}\omega t\right) , \tag{10}$$

where $G_\omega^*(x_j, 0|x_\mathrm{s}, L)$ is the conjugated monochromatic "Green's function" of the waveguide at frequency ω between a source at depth x_s and range L and a receiver at depth x_j and range 0. In other words, the phase-conjugated field in the plane of the source is the sum over the array elements of a product of two Green's functions: one describes the propagation from the source to the array, and the other describes the propagation from the array to the observation plane. Time reversal appears in the conjugation of the Green's function between the source and the array in the right term of (10). In a range-independent waveguide, the Green's function is expressed as follows:

$$G_\omega\left(x,0|x_\mathrm{s},L\right) = \frac{\mathrm{i}}{\rho\left(x_\mathrm{s}\right)\left(8\pi L\right)^{1/2}} \exp\left(-\mathrm{i}\frac{\pi}{4}\right) \sum_n \frac{u_n\left(x_\mathrm{s}\right) u_n\left(x\right)}{k_n^{1/2}} \exp\left(\mathrm{i}k_n L\right) , \tag{11}$$

where n is the number of the propagating mode, $u_n(x)$ corresponds to the modal shape as a function of depth and k_n is the wavenumber. To demonstrate that $\phi^{\mathrm{tr}}(x, y, t)$ focuses at the position of the initial source, we simply substitute (11) into (10), which specifies that we sum over all modes and array sources:

$$\phi^{\mathrm{tr}}\left(x,y,t\right) \approx \sum_j \sum_n \sum_m \frac{u_m\left(x\right) u_m\left(x_j\right) u_n\left(x_j\right) u_n\left(x_\mathrm{s}\right)}{\rho\left(x_j\right)\rho\left(x_\mathrm{s}\right)\sqrt{k_m k_n y L}} \exp\left[\mathrm{i}\left(k_m y - k_n L\right) - \omega t\right] . \tag{12}$$

For an array which substantially spans the water column, we approximate the sum of sources as an integral and invoke the orthonormality of the modes:

$$\int_0^\infty \frac{u_m\left(x\right) u_n\left(x\right)}{\rho\left(x\right)} \mathrm{d}x = \delta_{nm} . \tag{13}$$

The sum over j selects mode $m = n$, and (12) becomes

$$\phi^{\mathrm{tr}}\left(x,y,t\right) \approx \sum_m \frac{u_m\left(x\right) u_m\left(x_\mathrm{s}\right)}{\rho\left(x_\mathrm{s}\right) k_m \sqrt{yL}} \exp\left[\mathrm{i}k_m\left(y - L\right) - \omega t\right] . \tag{14}$$

In the plane of the source at $y = L$, the closure relations which define the modes as a complete set $\left(\sum_m \frac{u_m(x) u_m(x_\mathrm{s})}{\rho(x_\mathrm{s})} = \delta\left(x - x_\mathrm{s}\right)\right)$ can be applied

under the assumption that k_n are nearly constant over the interval of the contributing modes. This leads to $\phi^{\mathrm{tr}}(x, L, t) \approx \delta(x - x_{\mathrm{s}}) \exp(-\mathrm{i}\omega t)$, which proves that the phase-conjugated field focuses back at the source.

Kuperman et al. have experimentally demonstrated in the ocean the robustness of time-reversal focusing, provided the array adequately samples the field in the water column. They have shown that temporal changes in the ocean due to surface waves and internal waves degrade the focus but that this degradation is tolerable if the average Green's function is not severely perturbed by these time variations [17]. Moreover they experimentally achieved a shift of the focal range on the order of 10% by shifting the central frequency of the TRM prior to retransmission [18].

3.3 Time Reversal in Chaotic Cavities

In this section, we are interested in another aspect of multiply reflected waves: waves confined in closed reflecting cavities such as elastic waves propagating in a silicon wafer. With such boundary conditions, no information can escape from the system and a reverberant acoustic field is created. If, moreover, the cavity shows ergodic properties and negligible absorption, one may hope to collect all information at only one point. *Draeger* and *Fink* [19,20,21] have shown experimentally and theoretically that in this particular case a time reversal can be obtained *using only one time-reversal channel* operating in a closed cavity. The field is measured at one point over a long period of time and the time-reversed signal is re-emitted at the same position.

The experiment is 2-dimensional and is carried out by using elastic surface waves propagating along a monocrystalline silicon wafer whose shape is a chaotic stadium. The shape of the cavity is of crucial importance. The chaotic stadium geometry insures that each acoustic ray radiated by the source will pass, after several reflections, sufficiently close to any point of the cavity. This ergodic property may be obtained for different geometries, and the geometry called the "D-shape stadium" was chosen for its simplicity.

Silicon was selected for its weak absorption. The elastic waves which propagate in such a plate are Lamb waves. An aluminum cone coupled to a longitudinal transducer generates these waves at one point in the cavity. A second transducer is used as a receiver. The central frequency of the transducers is 1 MHz, and its bandwidth is 100%. At this frequency, only three Lamb modes are possible (one flexural, two extensional). The source is isotropic and considered point-like because the cone tip is much smaller than the central wavelength. A heterodyne laser interferometer measures the displacement field as a function of time at different points on the cavity. Assuming that there is nearly no mode conversion between the flexural mode and other modes at the boundaries, we have only to deal with one field, the flexural-scalar field.

The experiment is a two-step process as described above: In the first step, one of the transducers, located at point A, transmits a short omnidirectional signal of duration 0.5μs into the wafer. Another transducer, located at B,

observes a very long chaotic signal, which results from multiple reflections of the incident pulse along the edges of the cavity and which continues for more than 50 ms, corresponding to some one hundred reflections along the boundaries. Then, a portion of 2 ms of the signal is selected, time-reversed and re-emitted by point B. As the time-reversed wave is a flexural wave that induces vertical displacement of the silicon surface, it can be observed using the optical interferometer that scans the surface around point A (Fig. 9).

One observes both an impressive time recompression at point A and a refocusing of the time-reversed wave around the origin (Fig. 10), with a focal spot whose radial dimension is equal to half the wavelength of the flexural wave. Using reflections at the boundaries, the time-reversed wave field converges towards the origin from all directions and gives a circular spot, like the one that could be obtained with a closed time-reversal cavity covered with transducers. The 2-ms time-reversed waveform is the time sequence needed to focus exactly on point A.

The success of this time-reversal experiment is particularly interesting with respect to two aspects. Firstly, it proves again the feasibility of time

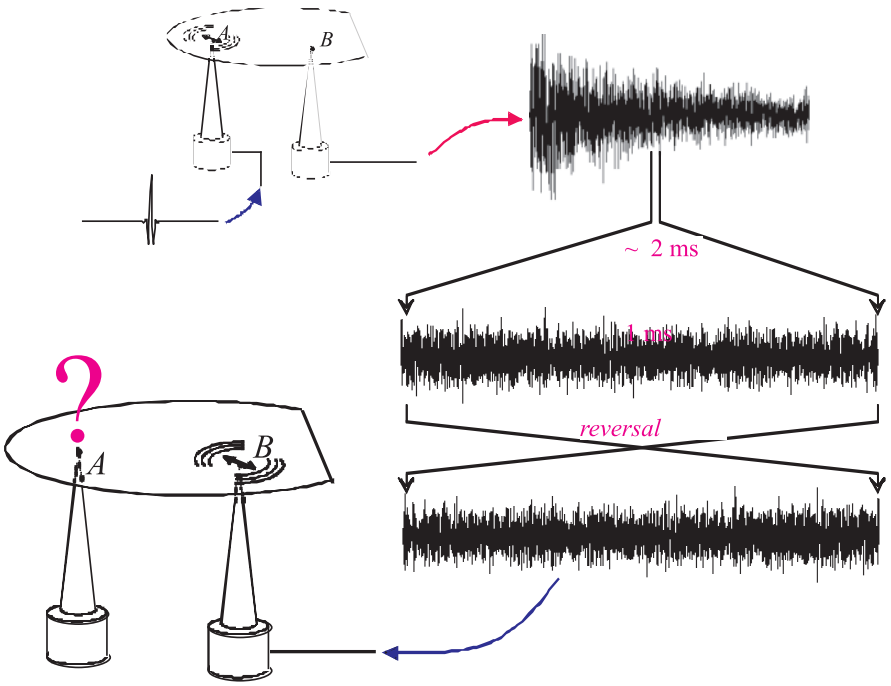

Fig. 9. In the first step, the transducer located at point A transmits a short omnidirectional signal ($0,5\mu$s) into the wafer. The transducer located at point B observes a very long chaotic signal which lasts more than 50 ms. In the second step, a portion of 2 ms of the signal is selected, time-reversed and re-emitted by point B

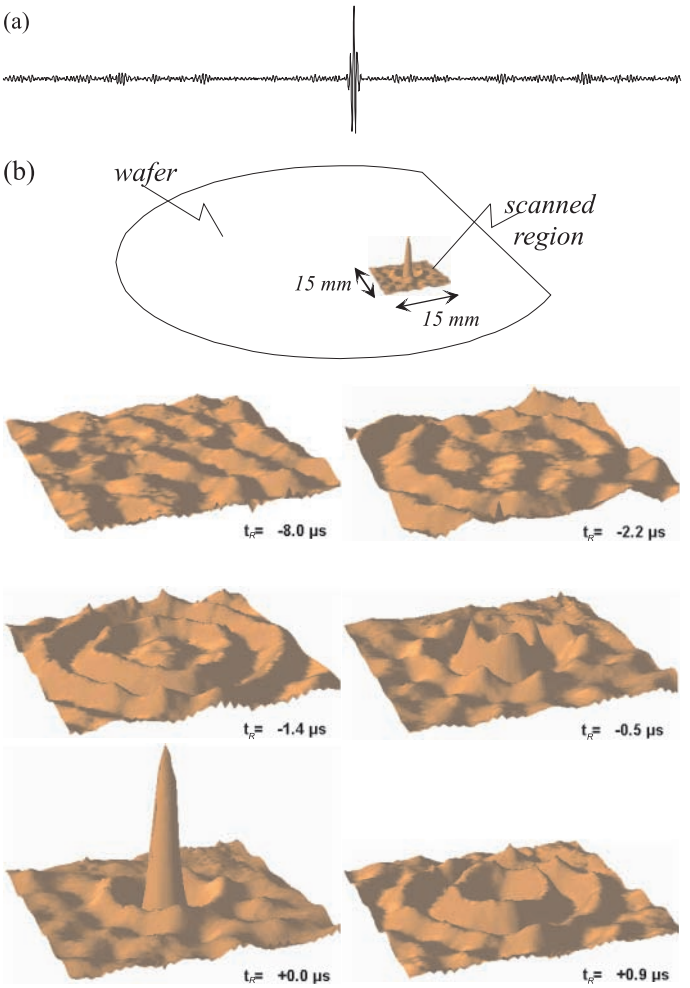

Fig. 10. (**a**) Time-reversed signal observed at point A. The observed signal is 210µs long. (**b**) Time-reversed wave field observed at different times around point A on a 15 mm × 15 mm square

reversal in wave systems with chaotic ray dynamics. Paradoxically, in the case of one-channel time reversal, chaotic dynamics is not only harmless but also even useful, as it guarantees ergodicity. Secondly, using a source of vanishing aperture, we obtain an almost perfect focusing quality. The procedure approaches the performance of a closed TRC, which has an aperture of 360°. Hence, a one-point time reversal in a chaotic cavity produces better results than a TRM in an open system. Using reflections at the edge, focusing quality is not aperture limited, and in addition, the time-reversed collapsing wavefront approaches the focal spot from all directions.

As for the multiple-scattering medium, focusing properties of the time-reversed wave can be calculated using the spatial correlator approach. Taking into account the modal decomposition of the impulse response $h_{\mathrm{AB}}(t)$ on the eigenmodes $\psi_n(\boldsymbol{x})$ of the cavity with eigenfrequency ω_n, we obtain

$$h_{\mathrm{AB}}(t) = \sum_n \psi_n(A)\psi_n(B)\frac{\sin(\omega_n t)}{\omega_n}\,, \quad (t>0)\,. \tag{15}$$

If $h_{A'B}(t)$ is the propagation impulse response from point B to an observation point A' (with coordinates $\boldsymbol{r}_1$), which is different from the source location A, the time-reversed signal recreated at A' at time $t_1 = 0$ can be written as follows:

$$\phi^{\mathrm{tr}}(\boldsymbol{r}_1, 0) = \int h_{AB}\,(t)\, h_{A'B}\,(t)\,\mathrm{d}t\,. \tag{16}$$

Thus the directivity pattern of the time-reversed wave field is given by the cross correlation of the Green's functions that can be developed on the eigenmodes of the cavity:

$$\phi^{\mathrm{tr}}(\boldsymbol{r}_1, 0) = \sum_n \frac{1}{\omega_n^2}\psi_n(A)\psi_n(\boldsymbol{r}_1)\psi_n^2(B)\,. \tag{17}$$

Note that in a real experiment one has to take into account the limited bandwidth of the transducers, so a spectral function $F(\omega)$ centered on frequency ω_{c}, with bandwidth $\Delta\,\omega$, must be introduced and we can write (17) in the form

$$\phi^{\mathrm{tr}}(\boldsymbol{r}_1, 0) = \sum_n \frac{1}{\omega_n^2}\psi_n(A)\psi_n(\boldsymbol{r}_1)\psi_n^2(B)F(\omega_n)\,. \tag{18}$$

Thus the summation is limited to a finite number of modes, which is typically in our experiment of the order of a few hundred. As we do not know the exact eigenmode distribution for each chaotic cavity, we cannot evaluate this expression directly. However, one may use a statistical approach and consider the average over different realizations, which consists of summing over different cavity realizations. So we replace in (18) the eigenmodes' product by their expectation values $\langle \ldots \rangle$. We also use the qualitative argument proposed by *Berry* [22,23,24] to characterize irregular modes in a chaotic system. If chaotic rays support an irregular mode, it can be considered as a superposition of a large number of plane waves with random direction and phase. This implies that the amplitude of an eigenmode has a Gaussian distribution with $\left\langle \psi_n^2 \right\rangle = \sigma^2$ and a short-range isotropic correlation function given by a Bessel function that can be written as follows:

$$\langle \psi_n(A)\psi_n(\boldsymbol{r}_1)\rangle = J_0(2\pi\,|\boldsymbol{r}_1 - \boldsymbol{r}_0|\,/\lambda_n)\,, \tag{19}$$

where λ_n is the wavelength corresponding to ω_n. If A and A' are sufficiently far apart from B not to be correlated, then

$$\left\langle \psi_n(A)\psi_n(\boldsymbol{r}_1)\psi_n^2(B)\right\rangle = \langle \psi_n(A)\psi_n(\boldsymbol{r}_1)\rangle \left\langle \psi_n^2(B)\right\rangle\,. \tag{20}$$

One obtains finally

$$\left\langle \phi^{\mathrm{tr}}(\boldsymbol{r}_1, 0) \right\rangle = \sum_n \frac{1}{\omega_n^2} J_0(2\pi \left| \boldsymbol{r}_1 - \boldsymbol{r}_0 \right| / \lambda_n) \sigma^2 F(\omega_n) \,. \tag{21}$$

The experimental results obtained in Fig. 10 agree with this prediction and show that in a chaotic cavity the spatial resolution is independent of the TRM aperture. Indeed, with a one-channel TRM, the directivity patterns at $t = 0$ are closed to the Bessel function $J_0(2\pi \left| \boldsymbol{r}_1 - \boldsymbol{r}_0 \right| / \lambda_{\mathrm{c}})$ corresponding to the central frequency of the transducers.

One can also observe that a very good estimate of the eigenmode correlation function is experimentally obtained with only one realization. A one-channel omnidirectional transducer is able to refocus a wave in a chaotic cavity, and we have not averaged the data on different cavities or on different positions of the transducer B.

3.3.1 Phase Conjugation Versus Time Reversal

This interesting result emphasizes how interesting time-reversal experiments are compared to phase-conjugated experiments. In phase conjugation, one only works with monochromatic waves and not with broadband pulses. For example, if one works only at frequency ω_n, so that there is only one term in (18), one cannot refocus a wave on point A. An omnidirectional transducer, located at any position B, working in monochromatic mode, sends a diverging wave in the cavity that has no reason to refocus on point A. The refocusing process works only with broadband pulses, with a large number of eigenmodes in the transducer bandwidth. Here, the averaging process that gives a good estimate of the spatial correlation function is not obtained by summing over different realizations of the cavity, as in (18), but by a sum over "pseudo-realizations" which correspond to the different modes in the same cavity. This come from the fact that in a chaotic cavity we may assume a statistical decorrelation of the different eigenmodes. As the number of eigenmodes available in the transducer bandwidth increases, the refocusing quality becomes better and the focal spot pattern becomes closed to the ideal Bessel function. Hence, the signal-to-noise level should increase as the square-root of the number of modes in the transducer bandwidth.

A similar result has also been observed in the time-reversal experiment conducted in a multiple-scattering medium. A clear refocusing has been obtained with only a single array element (Fig. 4). The focusing process works with broadband pulses (the transducer center frequency is 3.5 MHz with a 50% bandwidth at −6 dB). For each individual frequency there is no focusing, and the estimate of the spatial correlation is very noisy. However, for a large bandwidth, if we have statistical decorrelation of the wave fields for different frequencies, the time-reversed field is self-averaging.

4 Applications of Time-Reversal Mirrors

The most promising area for the application of TRMs is *pulse–echo* detection. In this domain, one is interested in the detection, imaging and sometimes destruction of passive reflecting targets. The low velocities of ultrasonic waves allows separation of reflecting targets at different depths. A piezoelectric transducer first sends a short impulse and then detects the various echoes from the targets. In nondestructive evaluation (NDE), cracks and defects can be found within materials of various shapes. In medical imaging, one looks for organ walls, calcification, tumors, kidney or gallbladder stones. In underwater acoustics, one looks for mines, submarines, or objects buried under sediments. In all of these cases, the acoustic detection quality depends on the availability of the sharpest possible ultrasonic beams to scan the medium of interest. The presence of an aberrating medium between the targets and the transducers can drastically change the beam profiles. In medical imaging, a fat layer of varying thickness, bone tissues, or some muscular tissues may greatly degrade focusing. In the human body, ultrasonic velocity variations from 1440 m/s in fat to 1675 m/s in collagen defocus and deflect acoustic beams. In NDE, the samples to be evaluated are usually immersed in a pool; the interface shape between the samples and the coupling liquid currently limits the detectability of small defects. In underwater acoustics, refraction due to oceanic structure ranging in scale from centimeters to tens of kilometers are important sources of distortions. For all these applications, a TRM array can be controlled according to a three-step sequence [25,26]. One part of the array generates a brief pulse to illuminate the region of interest through an aberrating medium. If the region contains a point reflector, the reflected wavefront is selected using a temporal window and the information acquired is time reversed and reemitted. The re-emitted wavefront refocuses on the target and through the aberrating medium. It compensates also for unknown array deformation. In terms of signal theory, time-reversal processing makes the spatio-temporally matched filter [27] to the propagation transfer function between the array and the target. Although this self-focusing technique is highly effective, it requires the presence of a reflecting target in the medium. When this medium contains several targets, the problem is more complicated and iteration of the time-reversal operation may be used to select one target. Indeed, if the medium contains two targets of different reflectivity, the time reversal of the echoes reflected from these targets generates two wavefronts focused on each target. The mirror produces the real acoustic images of the two reflectors on themselves. The highest amplitude wavefront illuminates the most reflective target, while the weakest wavefront illuminates the second target. In this case, the time reversal process can be iterated. After the first time-reversed illumination, the weakest target is illuminated more weakly and reflects a fainter wavefront than the one coming from the strongest target. After some iterations, the process converges and produces a wavefront focused on the most reflective target. It converges if the target separation is

sufficient to avoid the illumination of one target by the real acoustic image of the other one. *Prada* and *Fink* and *Prada* et al. [28,29] studied theoretically the convergence of time-reversal iterations in a multitarget medium and have determined the cases in which the target which reflects the most is selected among several targets. In some cases it is also interesting to learn how to focus on the other reflectors. The theoretical analysis of the iterative time-reversal process led to a very elegant solution to this problem (the DORT method), which is presented in Chap. 5. This analysis consists of determining the possible transmitted waveforms that are invariant under the time-reversal process. For these waveforms an iteration of the time-reversal operation gives stationary results. Such waveforms can be determined through the calculation of the eigenvectors of the so-called time-reversal operator.

Another interesting application of pulse–echo-mode TRMs is to put an elastic target in resonance. For example, if you illuminate an extended solid target with a short pulse, the backscattered field results in several contributions. A first reflected wave, "the specular echo," is determined by the target geometry. It is followed by a series of waves, "the resonant echo," which correspond to the propagation of surface and volume waves around and inside the scatterer. These waves are generated at particular points on the target. They propagate at the surface or in the solid, and they radiate into the fluid from different mode-conversion points on the scatterer, which behave as secondary sources. *Thomas* et al. [30] studied the case of a hollow target where the elastic part is mainly due to circumferential waves (dispersive Lamb waves): the first symmetrical and antisymmetrical Lamb waves, S_0 and A_0. As these two waves have different velocities, they can be separated experimentally by time windowing, and their generation points on the target are located at different positions in accordance with Snell's laws. Selecting and time reversing each wavefront separately, the time-reversed wave energy only concentrates at the generation points of the selected wave. This process enhances the generation of each specific Lamb wave compared to the other reflected waves. Iterating this process, we can build a waveform that is spatio-temporally matched to the vibration mode of the target. *Prada* et al. have extended the DORT technique [31] to this type of target, and they have demonstrated that each Lamb wave give rises to a set of eigenvectors of the time-reversal operator. These vectors can be calculated for a specific target and can be used to build optimal excitations of the array to put the target in resonance.

A first medical application of pulse–echo-mode TRMs is the destruction of kidney and gallbladder stones in the human body. Although the stones may be accurately located using X-ray imaging or ultrasonic scanners, it is difficult to focus precisely the ultrasonic waves in order to destroy the stones through inhomogeneous tissues. Furthermore, the stones move as much as several centimeters during breathing. Several thousand shots are required to destroy a stone and it is not currently possible to track the stone movements with a mechanical system. Consequently, it is estimated that, with current

piezoelectric devices, only 30% of the ultrasonic shots reach the stone. Ultrasonic time-reversal techniques can solve these problems. To locate a reflecting target, such as a kidney stone in its environment of other stones and organ walls, the zone of interest is illuminated using a few elements of the transducer matrix. The reflected signals are recorded with the whole matrix and time-reversed. When the process is iterated several times, the ultrasonic beam converges towards the area of the stone that reflects the most. The time-reversal iteration selects one of the spots. Once the spot has been reliably located, intermittent amplified pulses can be applied to shatter the stone. As the stone moves, the process is repeated in order to locate it in real time. With *Thomas* and *Wu* [32], we have developed a 64-channel TRM 20 cm in diameter.

Another major promise of self-focusing TRM arrays that has not yet been fulfilled is ultrasonic medical hyperthermia. In this technique, high-intensity ultrasound produces thermal effects. A part of the ultrasound energy is absorbed by the tissue and converted to heat, resulting in an increase in local temperature. If a temperature of 60–70 °C is reached, irreversible and deleterious effects will occur within several seconds. Focused ultrasound surgery pioneered in the 1950s by Fry at the University of Illinois did not gain general acceptance until recently [33,34]. Focal probes consisting of annular phased arrays are now marketed for the treatment of prostate cancer. These techniques are limited to the production of necrosis in tissues that are not moving; however, applications to abdominal and cardiac surgery are limited by the tissue motion induced both by the cardiac cycle and by breathing. At the University of Michigan, Ebbini and his group are developing self-focusing arrays to solve this problem. In our group, we are working on a TRM application for brain hyperthermia. The challenge of this application is to focus through the skull bone, which induces severe refractions and scattering of the ultrasonic beam. With Thomas and Tanter, we have shown that the porosity of the skull bone produces a strong dissipation, which breaks the time-reversal symmetry of the wave equation. We have shown [35,36] that time-reversal focusing is no longer appropriate to compensate for the skull properties, and we have developed a new focusing technique which combines a correction for the dissipative effects with classical time-reversal focusing. This technique allows us to focus and steer, through the skull, an ultrasonic beam which converges on a 1.5 mm diameter spot with very low side lobes.

Another important application of TRMs is flaw detection in solids. The detection of small defects is difficult when the inspected object consists of heterogeneous or anisotropic material and when the sample has a complex geometry. Usually, the solid and the ultrasonic transducers are immersed in water, and the transducers are moved to scan the zone of interest. Due to refraction, the ultrasonic beams can be altered by the water–solid interface. In addition, the longitudinally polarized ultrasound traveling in water may produce waves of different polarizations and velocities in the solid (longitudinal,

transverse and surface waves). Beam focusing and steering of the ultrasonic array in the solid is a difficult task for which self-focusing techniques have been proposed to enhance the flexibility of the process [37]. We have shown that using TRMs is a very effective technique to solve these problems. TRMs automatically compensate for refraction, mode conversion and anisotropy. In a joint program with SNECMA (Société Nationale d'Etudes et de Construction de Moteurs d'Avion), we have developed a 128-element TRM to detect the presence of low-contrast defects within titanium alloys used in jet engines. It is a difficult problem because titanium has a highly heterogeneous microstructure which produces large amounts of scattering noise that can hide the echo from a defect. With *Chakroun* et al. [38], we have shown that the iterative pulse–echo mode allows us to autofocus and to detect defects as small as 0.4 mm in 250-mm-diameter titanium billets. Compared to other techniques, the signal-to-noise ratio is enhanced in all situations, and smaller defects can be detected in the billet core, where ultrasonic beams are strongly distorted.

5 Conclusion

Time reversal has exciting applications in the field of acoustics. Because acoustic time-reversal technology is now easily accessible to modern electronic technology, it is expected that applications in various areas will expand rapidly. Initial applications show promise in medical therapy as well as in nondestructive testing. In addition to solving practical problems, time-reversal mirrors are also unique research tools that may allow us to better understand problems related to wave propagation in disordered media and reverberant cavities.

References

1. M. Fink, C. Prada, F. Wu, D. Cassereau, Self focusing in inhomogeneous media with time reversal acoustic mirrors, IEEE Ultras. Symp. Proc. **1**, 681–686 (1989) 17
2. M. Fink, Time reversal of Ultrasonic field-part I: Basic Principles, IEEE Trans. Ultrason. Ferroelec. Freq. Contr. **39**, 555–566 (1992) 17
3. M. Fink, Time Reversed Acoustics, Phys. Today **50**, 34–40 (1997) 17
4. D. R. Jackson, D. R. Dowling, Phase Conjugation in Underwater Acoustics, J. Acoust. Soc. Am. **89**, 171 (1991) 17, 18, 30
5. D. Cassereau, M. Fink, Time-reversal of ultrasonic fields, IEEE Trans. Ultrason. Ferroelec. Freq. Contr. **39**, 579–592 (1992) 18
6. J. de Rosny, M. Fink, submitted to Phys. Rev. Lett. 20
7. D. Cassereau, M. Fink, Time-reversal focusing through a plane interface separating two fluids, J. Acoust. Soc. Am. **96**, 3145–3154 (1994) 21
8. G. S. Kino, *Acoustics Waves* (Prentice Hall, Englewood Cliffs 1987) 21

9. A. Derode, P. Roux, M. Fink, Robust acoustic time-reversal with high order multiple scattering, Phys. Rev. Lett. **75**, 4206–4209 (1995) 21
10. R. Snieder, J. Scales, Time-reversed imaging as a diagnostic of wave and particle chaos, Phys. Rev. E **58**, 5668–5675 (1998) 24
11. A. Derode, A. Tourin, M. Fink, Limits of time-reversal focusing through multiple scattering: Long-range correlation, J. Acoust. Soc. Am. **107**, 2987 (2000) 26
12. A. Derode, A. Tourin, M. Fink, Ultrasonic pulse compression with one-bit time reversal through multiple scattering, J. Appl. Phys. **85**, 6343–6352 (1999) 27
13. P. Roux, B. Roman, M. Fink, Time-reversal in an ultrasonic waveguide, Appl. Phys. Lett. **70**, 1811 (1997) 27
14. A. Parvulescu, Matched signal ('MESS') processing by the ocean, J. Acoust. Soc. Am. **98**, 943 (1995) 30
15. A. Parvulescu, C. S. Clay, Reproductibility of signal transmissions in the ocean, Radio Elect. Eng. **29**, 233 (1965) 30
16. C. Feuillade, C. S. Clay, Source imaging and sidelobe suppression using time-domain techniques in a shallow water waveguide, J. Acoust. Soc. Am. **92**, 2165 (1992) 30
17. W. A. Kupperman, W. S. Hodgkiss, H. C. Song, T. Akal, T. Ferla, D. Jackson, Phase conjugation in the ocean: experimental demonstration of an acoustic time-reversal mirror, J. Acoust. Soc. Am. **103**, 25 (1998) 30, 32
18. W. Hodgkiss, H. Song, W. Kuperman, T. Akal, C. Ferla, D. Jackson, A long range and variable focus phase-conjugation experiment in shallow water, J. Acoust. Soc. Am. **105**, 1597 (1999) 30, 32
19. C. Draeger, M. Fink, One channel time-reversal of elastic waves in a chaotic 2D-silicon cavity, Phys. Rev. Lett. **79**, 407 (1997) 32
20. C. Draeger, M. Fink, One-channel time-reversal in chaotic cavities: theoretical limits, J. Acoust. Soc. Am. **105**, 618 (1999) 32
21. C. Draeger, M. Fink, One-channel time-reversal in chaotic cavities: experimental results, J. Acoust. Soc. Am. **105**, 611 (1999) 32
22. M. V. Berry, in Les Houches 1981 - *Chaotic Behaviour of Deterministic Systems* (North Holland, Amsterdam, 1983), p. 171 35
23. S. W. McDonald, A. N. Kaufman, Wave chaos in the stadium: Statistical properties of short-wave solutions of the Helmholtz equation, Phys. Rev. A **37**, 3067 (1988) 35
24. R. Weaver, J. Burkhardt, Weak Anderson localisation and enhanced backscatter in reverberation rooms and quantum dots, J. Acoust. Soc. Am. **96**, 3186 (1994) 35
25. C. Prada, F. Wu, M. Fink, The iterative time reversal mirror, J. Acoust. Soc. Am. **90**, 1119 (1991) 37
26. F. Wu, J.-L. Thomas, M. Fink, Time Reversal of Ultrasonic Fields—Part I: Experimental Results, IEEE Trans. Ultrason. Ferroelec. Freq. Contr. **39**, 567 (1992) 37
27. C. Dorme, M. Fink, Focusing in transmit-receive mode through inhomogeneous media: the time reversal matched filter approach, J. Acoust. Soc. Am. **98**, 1155 (1995) 37
28. C. Prada, M. Fink, Eigenmodes of the time reversal operator: a solution to selective focusing on two scatterers, Wave Motion **20**, 151 (1994) 38
29. C. Prada, J.-L. Thomas, M. Fink, The iterative time-reversal process: analysis of the convergence, J. Acoust. Soc. Am. **97**, 62 (1995) 38

30. J.-L. Thomas, P. Roux, M. Fink, Inverse problem in wave scattering with an acoustic time reversal mirror, Phys. Rev. Lett. **72**, 637–640 (1994) 38
31. C. Prada, J.-L. Thomas, P. Roux, M. Fink, Acoustic time reversal and inverse scattering, in H. D. Bui, M. Tamaka (Ed.), *Inverse problems in engineering mechanics*, Proc. 2nd Int. Symp. Inv. Prob. at Paris, Nov 2–4, 1994 (Balkema, Rotterdam 1994) pp. 309–316 38
32. J.-L. Thomas, F. Wu, M. Fink, Time Reversal Mirror applied to litotripsy, Ultras. Imag. **18**, 106 (1996) 39
33. L. Crum, K. Hyninen, Sound Therapy, Phys. World, 28, August (1996) 39
34. H. Wang, E. S. Ebinni, M. O. Donell, C. A. Cain, Phase aberration correction and motion compensation for ultrasonic hyperthermia phased arrays: experimental results, IEEE Trans. Ultrason. Ferroelec. Freq. Contr. **41**, 34 (1994) 39
35. J.-L. Thomas, M. Fink, Ultrasonic beam focusing through tissue inhomogeneities with a time reversal mirror: Application to transkull therapy, IEEE Trans. Ultrason. Ferroelec. Freq. Contr. **43**, 1122 (1996) 39
36. M. Tanter, J.-L. Thomas, M. Fink, Focusing and steering through absorbing and heterogeneous medium: application to ultrasonic propagation through the skull, J. Acoust. Soc. Am. **103**, 2403 (1998) 39
37. B. Beardsley, M. Peterson, J. D. Achenbach, A simple scheme for self-focusing of an array, J. Nondestr. Eval. **14**, 169 (1995) 40
38. N. Chakroun, M. Fink, F. Wu, Time reversal processing in non destructive testing, IEEE Trans. Ultrason. Ferroelec. Freq. Contr. **42**, 1087 (1995) 40

Index